New gravitational wave probe of vector dark matter

Alisha Marriott-Best[a] [1], Marco Peloso[b] [2], Gianmassimo Tasinato[a,c] [3]

[a] *Physics Department, Swansea University, SA2 8PP, United Kingdom*
[b] *Dipartimento di Fisica e Astronomia, Università degli Studi di Padova, INFN, Sezione di Padova, via Marzolo 8, I-35131 Padova, Italy*
[c] *Dipartimento di Fisica e Astronomia, Università di Bologna, INFN, Sezione di Bologna, I.S. FLAG, viale B. Pichat 6/2, 40127 Bologna, Italy*

Abstract

The longitudinal components of massive vector fields generated during inflation constitute a well-motivated dark matter candidate, with interesting phenomenological implications. During the epoch of radiation domination following inflation, their spectrum exhibits a peak at small scales, whose amplitude and position are governed by the parameters of the dark matter model. We calculate the stochastic gravitational wave spectrum induced at second order in fluctuations by such a longitudinal vector peak. We demonstrate that the amplitude of the gravitational wave spectrum can, in principle, reach significant values at nano-Hertz frequencies or lower. This result suggests a novel gravitational wave probe to test inflationary vector dark matter scenarios, independent from assumptions on the coupling of dark vectors to the Standard Model. Additionally, we derive new analytical formulas for the longitudinal vector transfer functions during radiation domination, offering a valuable tool for characterising the convolution integrals that govern the properties of the induced gravitational waves.

1 Introduction

Determining the nature of dark matter (DM) is one of the most pressing open questions in physics. If DM is a particle, it should couple very feebly to the Standard Model (SM) of particle physics, as only its gravitational interactions with normal matter have been observed so far [1,2]. It is possible for DM particles to have no gauge interactions at all with the SM; at most, they may have kinetic mixings or interactions with gauge singlets. In this case, we can reveal its presence through so-called DM portals, see e.g. [3,4] for reviews. In this work we discuss a new gravitational wave probe of certain well-motivated models of particle DM.

We consider the framework developed in [5] where DM consists of the longitudinal components of a massive dark photon and is produced via gravitational effects during the inflationary epoch. Gravitational production of scalar fields in the context of inflationary scenarios has previously been investigated (see [6–8]). Ref. [5] extended these analyses to the spin-1 case, establishing a connection to DM. Specifically, it highlighted the role of the longitudinal component induced by the mass term, whose Lagrangian in a Friedmann–Lemaître–Robertson–Walker (FLRW) background was first provided and analysed in [9]. The scenario proposed in [5] has been further

[1] 2347066.at.swansea.ac.uk
[2] marco.peloso.at.infn.it
[3] g.tasinato2208.at.gmail.com

examined and expanded in various theoretical studies, such as [10–21]. Its potential phenomenological implications have been explored in works such as [22–32].

When evaluated during radiation domination, the resulting momentum-dependent spectrum of longitudinal vector modes exhibits a peak at small scales relative to the CMB. The amplitude and position of this peak depend on the vector mass and other defining model parameters (see Figure 1). We compute the second-order gravitational waves (GWs) induced by this peak in isocurvature longitudinal modes. The resulting stochastic gravitational wave background (SGWB) serves as a distinctive signature, offering a potential probe of a mechanism where DM interacts with the SM solely through gravity, making it undetectable except via its gravitational effects. If observed, the predicted momentum dependence of this GW signal would serve as a smoking gun for this scenario.

Induced GWs generated by enhanced adiabatic modes during inflation have been extensively studied [33–39]. For a comprehensive review, see [40], as well as [41], for a recent account. This possibility is particularly well-motivated in models that produce primordial black holes (PBHs), as highlighted in the survey [42]. In particular, the viable sub-lunar mass range where PBHs could constitute the entirety of DM corresponds to a GW signal that would be distinctly observable by LISA [43, 44]. Second-order GWs arising from isocurvature fluctuations have also been investigated, and discussed in [45–47].

In this work, we explore the novel scenario where the sourcing perturbations are fluctuations in the longitudinal mode of a massive vector field. Specifically, in Section 2, we review the framework of [5] and examine potential generalisations, introducing new analytical approximations for the transfer functions of the longitudinal vector mode during radiation domination. In Section 3, we compute the spectrum of induced GWs in this regime, demonstrating that it exhibits a broad peak at frequencies determined by the position of the longitudinal vector spectrum peak. Finally, in Section 4, we discuss the phenomenological implications for GW physics.

Regardless of the actual realisation or extension of the ideas introduced in [5], if the longitudinal vector modes constitute all of DM, we find a well specific relation between the amplitude of the GW spectrum and the position of its peak, scaling as

$$\frac{\Omega_{\rm GW}^{\rm peak}}{10^{-10}} \simeq \left(\frac{f_{\rm peak}}{10^{-10}\,{\rm Hz}}\right)^{-2} .$$

We discuss how this 'consistency relation' indicates that the induced GW spectrum can be measured if we have sufficient sensitivity to GW at nano-Hz scales, or below. We conclude with an outlook in Section 5.

2 Longitudinal vector dark matter from inflation

We begin with a review of the ideas developed in [5], which propose a scenario for DM in terms of longitudinal vector modes produced during inflation. We emphasise aspects which will be relevant for our later discussion of the SGWB induced by vector longitudinal fluctuations. We present new results concerning analytical fits for transfer functions of the longitudinal vector components during radiation domination.

We consider a system based on a massive vector field minimally coupled with gravity. The

action is:

$$S = \int \sqrt{-g}\left[\frac{R}{2} - \frac{1}{4}F_{\mu\nu}F^{\mu\nu} - \frac{M^2}{2}A_\mu A^\mu\right], \tag{2.1}$$

where we have set $M_{\rm Pl} = 1$ unless otherwise stated; $F_{\mu\nu} = \partial_\mu A_\nu - \partial_\nu A_\mu$ is the vector field strength, and M^2 its mass squared, that we assume to be positive to avoid ghosts [9]. We consider a FLRW geometry, with scale factor a plus transverse and traceless tensor perturbations (GW):

$$ds^2 = a^2(\tau)\left[-d\tau^2 + (\delta_{ij} + h_{ij})\,dx^i dx^j\right]. \tag{2.2}$$

Finally, we assume that the vector field has a vanishing background value, and we parametrise its fluctuations as

$$A_\mu = \left(A_0,\, \partial_i\varphi + A_i^T\right). \tag{2.3}$$

The A_0 component is a constrained field whose evolution (as detailed below) is governed by the dynamics of the component φ, referred to as the *longitudinal scalar component*. The field A_i^T is the transverse vector component, which is only gravitationally coupled to the longitudinal one, and plays no relevant role in our study [5]. We note that the above line element neglects the scalar fluctuations of the metric, under the assumption that they provide subdominant contributions to the dynamics of the longitudinal vector modes. Such hypothesis is motivated by the fact that they are not amplified by the mechanism we are going to review next. We note that we are therefore assuming that the longitudinal vector fluctuations are non-adiabatic.

It is convenient to work in Fourier space, where the spatial part of (2.3) can be written as the sum $\vec{A} = \vec{A}^T + \hat{k}A_L$ of a transverse $\vec{A}^T$ and of a longitudinal vector component A_L, with

$$A_L = i\,k\,\varphi\,. \tag{2.4}$$

The temporal component A_0 appears in the action without time derivatives. In Fourier space, its equation of motion is algebraic in this variable, allowing A_0 to be expressed in terms of φ (or equivalently, A_L) without introducing a new dynamical degree of freedom.

$$A_{0\,\mathbf{k}} = \frac{k^2}{k^2 + M^2a^2}\,\varphi'_{\mathbf{k}} = \frac{-i\,k}{k^2 + M^2a^2}\,A'_{L\,\mathbf{k}}\,, \tag{2.5}$$

where prime denotes differentiation with respect to conformal time. We substitute this expression into the quadratic action for the longitudinal scalar fluctuations in Fourier space and obtain the action for the longitudinal degree of freedom on a FLRW background [9]

$$S = \int d\tau d^3k\,\frac{k^2a^2(\tau)}{2}\left[\frac{M^2}{k^2 + M^2a^2(\tau)}\varphi'_{\mathbf{k}}\varphi'_{-\mathbf{k}} - M^2\varphi_{\mathbf{k}}\varphi_{-\mathbf{k}}\right]. \tag{2.6}$$

The longitudinal scalar variable φ has a non-canonical kinetic structure – a consequence of the procedure of integrating out the auxiliary field A_0. The corresponding equation of motion reads

$$\varphi''_{\mathbf{k}} + \frac{2k^2\,aH}{k^2 + a^2M^2}\varphi'_{\mathbf{k}} + (k^2 + M^2a^2)\,\varphi_{\mathbf{k}} = 0\,. \tag{2.7}$$

Building on [5,11,13,14], we solve this equation during inflation, and during the following radiation dominated era. For this study, it is convenient to introduce the canonically normalised mode

$$\pi_{\mathbf{k}} \equiv \frac{kMa}{\sqrt{k^2 + a^2\,M^2}}\varphi_{\mathbf{k}}\,. \tag{2.8}$$

Substituting this relation, the action (2.6) takes the form

$$S = \frac{1}{2}\int d\tau d^3k \left[\pi'_{\mathbf{k}}\pi'_{\mathbf{k}} - \left(k^2 + a^2M^2 + \frac{3k^2M^2a'^2}{\left(k^2+a^2M^2\right)^2} - \frac{k^2}{k^2+a^2M^2}\frac{a''}{a}\right)\pi_{\mathbf{k}}\pi_{-\mathbf{k}}\right] , \tag{2.9}$$

where a boundary term has been subtracted to eliminate terms with a single time derivative acting on the mode.

2.1 Evolution during inflation

We assume that standard slow-roll inflation is driven by an additional field independent of the vector sector under consideration. Details of this sector are not required for our study — neither at the level of the background evolution nor at the level of fluctuations. Moreover, we can work to leading order in the slow-roll approximation, assuming a de Sitter expansion during inflation with a constant Hubble parameter H_I. We also assume the inequality

$$\frac{M}{H_I} \ll 1 , \tag{2.10}$$

relating the vector mass entering the action (2.1), and the inflationary Hubble parameter.

As demonstrated in [5], for very small M the late-time spectrum of longitudinal perturbations during radiation domination exhibits a peak at the scales $k = a_* M$, where a_* is the scale factor when the Hubble rate (well after inflation) is equal to M. Consequently, for all the scales of our interest, the condition $aM \ll k$ holds throughout inflation, both in the sub-horizon ($k \gg aH_I$) and super-horizon ($k \ll aH_I$) regimes. Namely, we consider the inequalities

$$\text{subhorizon :} \qquad \frac{k}{a\,H_I} \gg 1 \gg \frac{M}{H_I} , \tag{2.11}$$

and

$$\text{superhorizon :} \qquad \frac{M}{H_I} \ll \frac{k}{a\,H_I} \ll 1 , \tag{2.12}$$

all throughout inflation. Meaning the redefinition (2.8) can be approximated as

$$\pi_{\mathbf{k}} \simeq a\,M\,\varphi_{\mathbf{k}} . \tag{2.13}$$

and the canonical action (2.9) is well approximated by setting $M = 0$ in the equation. In doing so the standard action of a free massive field in de Sitter is obtained, which then provides the two point correlation function at super-horizon scales (see e.g. [48])

$$\langle \pi_{\mathbf{k}}\pi_{\mathbf{k}'}\rangle = \frac{a^2H_I^2}{2k^3}\delta^{(3)}\left(\mathbf{k}+\mathbf{k}'\right) \equiv \frac{2\pi^2}{k^3}\mathcal{P}_\pi\left(k\right) , \tag{2.14}$$

where the final expression is the standard definition of the power spectrum (in the following, we use an identical relation for the power spectra of other field variables). From the rescalings (2.13) and (2.4) we obtain the super-horizon power spectra [5]:

$$\mathcal{P}^{(0)}_{\varphi}\left(k\right) = \frac{H_I^2}{4\pi^2\,M^2} \quad \Rightarrow \quad \mathcal{P}^{(0)}_{A_L}\left(k\right) = \frac{k^2}{M^2}\frac{H_I^2}{4\pi^2} , \tag{2.15}$$

where the suffix (0) has been added to indicate that these quantities are constant, and they provide initial conditions for the mode evolution during the radiation dominated era. The primordial spectrum for the longitudinal scalar φ is scale invariant, where the amplitude is controlled by the vector mass and the inflationary Hubble parameter. In contrast the primordial spectrum of the longitudinal vector A_L grows as k^2 during inflation [5] – recall the relation (2.4). This scale dependence allows us to avoid CMB isocurvature constraints at (large) CMB scales. However, during radiation domination, the spectrum is not a monotonic function of k and instead develops a peak, as we will review in Section 2.2.

While Eq. (2.15) is the result of the minimal scenario proposed in [5], it is possible to generalise the original idea along various directions. Beyond their intrinsic interest, generalisations are particularly relevant for the study of induced gravitational waves – see Sections 3 and 4. In fact, only extensions of [5] can produce a gravitational wave spectrum with a sufficiently large amplitude to be detectable by gravitational wave experiments.

In the literature, attempts to generalise [5] move along different directions, by

1. Including reheating effects, or changes in cosmological history between the phases of de Sitter inflation and the onset of radiation domination, see e.g. [11, 13, 14]. In this case, the evolution of mode functions depend on the early cosmological evolution, which influences the amplitude and scale dependence of the vector energy density during radiation domination.

2. Considering non minimal couplings to gravity during inflation, see e.g. [21, 49], as well as the review [50]. For example, a ghost-free vector coupling with the Einstein tensor as $\alpha\, A^\mu A^\nu\, G_{\mu\nu}$, controlled by a constant α, leads to a longitudinal scalar spectrum amplitude $\mathcal{P}_\varphi^{(0)} = H_I^2/\left(4\pi^2\, \left(M^2 + \alpha^2\, H_I^2\right)\right)$ during inflation [21].

3. Envisaging mechanisms as phase transitions that change the value of the vector mass during inflation, or immediately after such phase; see e.g. [15] for an explicit construction. If the change of mass happens while the mass is much smaller than the Hubble rate and the physical momentum of a given mode, the vector mode function (and its time derivative) do not change in any appreciable way. However, as we show below, the vector energy density and its coupling to the gravitational waves increase if the vector mass increases, and, as seen for instance from eqs. (2.31) and (3.27), a change of the mass has the exact same effect as a change in the amplitude of the primordial longitudinal spectrum whilst the mode is well outside the horizon. So, we can mathematically treat this case analogously to the two previous ones.

We stress that extensions of the original model [5] are expected to introduce some degree of specific scale dependence in the spectrum of longitudinal vector modes. However, since our focus is not on specific model building, we assume - both for simplicity and phenomenological reasons - that such generalisations only modify overall normalisation of the longitudinal mode spectrum at the onset of radiation domination. Namely, we assume that Eq. (2.15) is generalised to the formula

$$\mathcal{P}_\varphi^{(0)}(k) \,=\, \sigma_0\, \frac{H_I^2}{4\pi^2\, M^2}\,, \tag{2.16}$$

where σ_0 is a constant dependent on specific scenarios that go beyond [5]. For our purposes, we assume σ_0 is a free parameter. As explained above, it will play an important role for the considerations in Section 4.

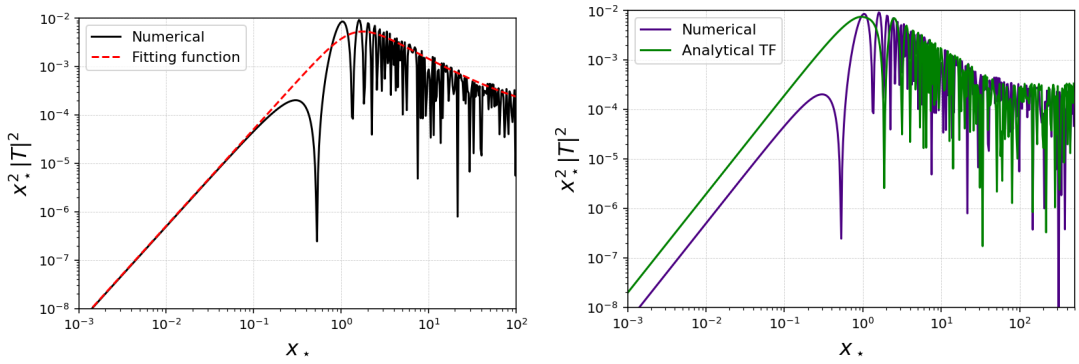

Figure 1: Representation of the longitudinal mode spectrum $(2\pi M)^2/(\sqrt{\sigma_0}\,k_\star\,H_I)^2\,\mathcal{P}_{A_L} = x_\star^2\,|T|^2$. **Left Panel:** Numerical approach. We evaluate this quantity at time $y_{fin} = 55$, while $y_{in} = 10^{-3}$. In red dashed the fitting function (2.24). See Section 2.2. **Right Panel:** Numerical versus analytical spectrum using the analytical transfer functions in RD as developed in Section 2.3.

2.2 Evolution during radiation domination

We take Eq. (2.16) as reference for the initial primordial spectrum and evolve it during radiation domination (RD). This is done by using transfer functions and expressing Eq. (3.10) during RD ($\tau \geq 0$) as

$$\varphi_{\mathbf{k}}(\tau) \;=\; T(k\tau)\,\varphi_{\mathbf{k}}^{(0)}\,, \tag{2.17}$$

with $\varphi_{\mathbf{k}}^{(0)}$ the initial value of the longitudinal scalar leading to the spectrum in Eq. (2.16). We follow the approach [4] outlined in [21] to handle the transfer functions.

Using Eq. (2.7), we find that the transfer function of Eq. (3.10) obeys the following evolution equation during RD:

$$T''(x) + \frac{2}{x}\left(1+\frac{a^2\,M^2}{k^2}\right)^{-1} T'(x) + \left(1+\frac{a^2\,M^2}{k^2}\right) T(x) \;=\; 0\,, \tag{2.18}$$

where prime denotes differentiation with respect to $x \equiv k\tau$, and we impose $T \to 1$ at superhorizon scales $x \ll 1$. The mass M indicates the vector mass during RD. In this era, $aH = 1/\tau$. The Hubble rate decreases with respect to the inflationary value H_I, a_* denotes the value of the scale factor when the rate becomes equal to the vector mass,

$$H_\star \;\equiv\; H(a_\star) \;=\; M \tag{2.19}$$

It is convenient to define the pivot scale

$$k_\star \equiv a_\star M\,. \tag{2.20}$$

As we will review next, $k_\star$ marks a turning point in the slope of the longitudinal vector spectrum profile during RD, where the slope transitions from increasing to decreasing as a function of momentum. We introduce the notation

$$x \;\equiv\; k\tau \quad ; \quad y \equiv \frac{x}{x_\star} \quad ; \quad x_\star \equiv \frac{k}{k_\star}\,. \tag{2.21}$$

[4] GT thanks Ogan Özsoy for collaborating on [21] and for providing key insights in the treatment of transfer functions.

Recall that $a \propto \tau$ during RD, hence we can write $y = a/a_\star$. Since $dy/dx = 1/x_\star$, in terms of these variables the evolution of the transfer function reads

$$\frac{d^2T(y)}{dy^2} + \frac{2\,(1+y^2/x_\star^2)^{-1}}{y}\,\frac{dT(y)}{dy} + (x_\star^2 + y^2)\,T(y) \;=\; 0\,. \tag{2.22}$$

This is numerically integrated for a set of different values $x_\star = k/k_\star$, which correspond to different comoving momenta normalised to the pivot momentum k_*. For each integration, we impose the initial conditions $T(y_{\rm in}) = 1$, $\frac{dT(y_{\rm in})}{dy} = 0$, with [5] $y_{\rm in} \equiv a_{\rm in}/a_\star \equiv \sqrt{M/H_I}$. The result is evaluated at a sufficiently late time, when $y_f = \frac{a_f}{a_*}\,{\rm e}^4$, when the longitudinal spectrum stabilises its shape as a function of frequency.

The resulting spectrum of longitudinal modes A_L during RD at time y_f is

$$\mathcal{P}_{A_L}(k, y_f) \;=\; \left(\frac{\sqrt{\sigma_0}\,k_\star\,H_I}{2\pi M}\right)^2 \frac{k^2}{k_\star^2}\,|T(x_\star, y_f)|^2\;. \tag{2.23}$$

The left panel in Fig 1 is a numerical evaluation of this spectrum, where it is normalised versus $(\sqrt{\sigma_0}\,k_\star\,H_I)^2/(2\pi M)^2$, with the σ_0 the factor defined in Eq. (2.16). Notice that, as anticipated, the spectrum changes slope at around $x_\star = 1$, i.e. for scales $k \sim k_\star$. In the same figure we also represent an analytical fitting function

$$\begin{aligned}\frac{(2\pi M)^2}{(\sqrt{\sigma_0}\,k_\star\,H_I)^2}\,\mathcal{P}_{A_L}(k, y_{\rm fin}) \;&=\; x_\star^2 |T(x_\star, y_{\rm fin})|^2 \\ &=\; 10^{-2}\left(\frac{x_\star}{1.4}\right)^2\left[1+\left(\frac{x_\star}{1.4}\right)^3\right]^{-1} + 10^{-4}\left(\frac{x_\star}{10}\right)^2\left[1+\left(\frac{x_\star}{10}\right)^2\right]^{-1}\,,\end{aligned} \tag{2.24}$$

indicating that the spectrum increases as $(k/k_\star)^2$ from large to small scales, reaching a maximum at $k \sim k_\star$, then decreases as $(k/k_\star)^{-1}$, and finally stabilises to a constant value at very small scales. This behaviour is consistent with the results of [5].

Numerical analysis demonstrates that the longitudinal vector spectrum has a peak at small scales during RD – a noteworthy feature that can produce induced GW at second order in fluctuations. However, beyond numerics, it is desirable to have better analytical control over the transfer function for the longitudinal scalar during RD. Which we address in the next session.

2.3 New analytic approach to the transfer function

The evolution equation (2.22) for the transfer functions during RD has analytical solutions in the regimes [6] of small and large y.

Small $y/x_\star$: The solution of (2.22), using the same definition of $y_{\rm in}$ and the appropriate initial conditions, is given by

$$T(y) \;=\; \frac{\sin\left[x_\star\,(y - y_{\rm in})\right]}{x_\star y} + \frac{y_{\rm in}\cos\left[x_\star\,(y - y_{\rm in})\right]}{y}\,, \tag{2.25}$$

[5] Since $H \propto t^{-1} m \propto a^{-2}$ during RD, the choice $y_{\rm in} \equiv \sqrt{M/H_I}$ corresponds to $H_{\rm in} = H_*\,(a_*/a_{\rm in})^2 = H_I$. Namely, the variable y evaluates to $y_{\rm in}$ at the onset of RD, which in this computation is assumed to occur right after the end of inflation.

[6] Recall the definitions of y and $x_\star$ in Eq. (2.21).

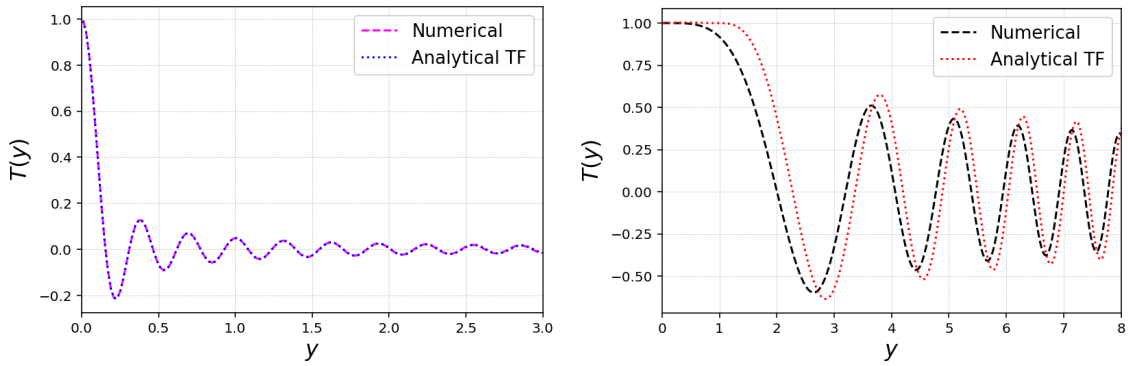

Figure 2: **Left panel** Numerical solution of transfer function in the small $y/x_\star$ regime (magenta), versus the analytical solution (2.25) (blue). We choose $x_\star = 20.3$. **Right panel** Numerical solution of transfer function in the large $y/x_\star$ regime (black), versus the analytical solution (2.26) (red). We choose $x_\star = 0.01$.

Large $y/x_\star$: The solution is

$$T(y) \;=\; c_1\, D_{-1/2}\left[(1+i)y\right] + c_2\, D_{-1/2}\left[-(1+i)y\right]\,, \tag{2.26}$$

with $D_\nu[z]$ the parabolic cylinder function, and the constants $c_{1,2}$ are fixed by boundary conditions.

Using asymptotic formulas for the cylinder functions, we determine a convenient approximation, which is reasonably accurate for all values of y and $x_\star$. It is defined in two regimes of $x_\star$ (from now on we set for simplicity $y_{\rm in} = 0$):

1. Range $x_* \ll 1$

$$\begin{aligned} T_{\rm early} &= \frac{\sin\left(x_* y\right)}{x_* y} && \text{valid for } y \ll 1\,, \\ T^{(A)}_{\rm late} &= \frac{1}{\sqrt{y}}\left[c_1^A\,\cos\left(\frac{y^2}{2}\right) + c_2^A\,\sin\left(\frac{y^2}{2}\right)\right] && \text{valid for } y \gg 1\,, \end{aligned} \tag{2.27}$$

with

$$\begin{aligned} c_1^A &= -\sin\left(1/2\right)\,\cos x_* + \left(\cos\left(1/2\right) + \frac{1}{2}\sin\left(1/2\right)\right)\,\frac{\sin x_*}{x_*}\,, \\ c_2^A &= \cos\left(1/2\right)\,\cos x_* + \left(\sin\left(1/2\right) - \frac{1}{2}\cos\left(1/2\right)\right)\,\frac{\sin x_*}{x_*}\,. \end{aligned} \tag{2.28}$$

2. Range $x_* \gg 1$

$$\begin{aligned} T_{\rm early} &= \frac{\sin\left(x_* y\right)}{x_* y} && \text{valid for } y \ll x_\star\,, \\ T^{(B)}_{\rm late} &= \frac{1}{\sqrt{y}}\left[c_1^B\,\cos\left(\frac{y^2}{2}\right) + c_2^B\,\sin\left(\frac{y^2}{2}\right)\right] && \text{valid for } y \gg x_\star\,, \end{aligned} \tag{2.29}$$

with

$$c_1^B \simeq \frac{\sin\left(x_*^2/2\right)}{x_*^{3/2}}\left(1+\frac{\sin x_*^2}{2x_*^2}\right),$$
$$c_2^B \simeq \frac{\cos\left(x_*^2/2\right)}{x_*^{3/2}}\left(1-\frac{\sin x_*^2}{2x_*^2}\right). \tag{2.30}$$

We extend the region of validity of the above expressions (2.27) and (2.29) to include also the transition regions at $y = 1$ and $x_* = 1, y$, by replacing the strong inequalities $\ll$ and $\gg$ with, respectively, $\leq$ and $\geq$. The above choice of the $y-$independent coefficients $c_{1,2}^{A/B}$ makes this analytic approximation for T, as well as its derivatve $\frac{\partial T}{\partial y}$ continuous across the transition regions. In Fig 2 we compare our analytical approximation of the transfer functions against numerics for two representative values of $x_\star$. Numerical checks show that our previous formulas (2.27) and (2.29) give reasonably accurate results also for intermediate values of $x_\star$. In Fig 1, right panel, we compare the longitudinal mode spectrum as function of scale $x_\star = k/k_\star$, computed with our analytical transfer functions against numerics. The profile (and the maximum) of the spectrum are captured quite well – in particular the position and amplitude of the peak, the spectral slope, as well as the oscillatory behaviour towards small scales.

In fact, in deriving Eqs (2.27) and (2.29) we make an effort to catch the oscillatory behaviour of the transfer functions. The latter plays an important role in the convolution integrals of Section 3 for the computation of the induced GW spectrum. As the present work was being completed, similar examples of transfer functions have appeared in [51] in a related (but not identical) context.

2.4 The energy density in the longitudinal vector mode

The computation of the energy density ρ_{A_L} stored in the longitudinal vector field is a useful first application of the analytic formulas derived in Section 2.3. The quantity ρ_{A_L} is extracted from the time-time component of the vector energy momentum tensor. It is given by [5]:

$$\rho_{A_L} = \frac{M^2}{2a^2}\int d\ln k\left[\frac{\mathcal{P}_{(\partial_\tau A_L)}}{k^2+a^2M^2}+\mathcal{P}_{A_L}\right], \tag{2.31}$$

with M the vector mass during RD. Substituting expression (2.15) for the primordial longitudinal vector spectrum (including the σ_0 factor of Eq. (2.16)), and using the transfer functions, this expression becomes

$$\rho_{A_L} = \frac{\sigma_0 H_I^2}{8\pi^2 a^2}\frac{a_\star k_\star^2}{a}\left[\int d\ln k\left(\frac{k^2 a}{a_\star k_\star^2(k^2+a^2M^2)}|\partial_\tau T|^2+\frac{a\,k^2}{a_\star k_\star^2}|T|^2\right)\right]. \tag{2.32}$$

In passing from Eq. (2.31) to Eq. (2.32), we acquire a factor proportional to $4\pi^2 M^2\mathcal{P}_\varphi^{(0)}/H_I^2$. In the original scenario [5], this factor is equal to one (see Eq. (2.15)). Due to the fact that the primordial inflationary spectrum is proportional to the inverse of the square of the vector mass during inflation (recall the arguments leading to Eq. (2.15)); when considering more general models, for example where the vector mass during inflation has value $m_{\rm inf}$ (which is different from the RD vector mass M). This factor leads to an effective overall constant $\sigma_0 = M^2/m_{\rm inf}^2$ in Eq. (2.32). Effectively, in this particular case, this phenomenon is captured by the factor σ_0

in Eq. (2.16). More generally, in what follows – without focussing on specific scenarios – we keep the parameter σ_0 as free constant in Eq. (2.32).

We focus on the dimensionless integral inside the square bracket in formula (2.32)

$$\mathcal{I}_\rho(y) = \int d\ln k \left[\frac{k^2\, a}{a_\star\, k_\star^2 (k^2 + a^2 M^2)} |\partial_\tau T|^2 + \frac{a\, k^2}{a_\star\, k_\star^2} |T|^2\right] \tag{2.33}$$

$$= y \int d\ln x_\star \left[\frac{x_\star^2}{x_\star^2 + y^2} |\partial_y T|^2 + x_\star^2 |T|^2\right], \tag{2.34}$$

where in the second line we pass to the dimensionless 'time' coordinate y introduced in Eq. (2.21). We evaluate this integral at late times, which we denote with $y = y_{\rm end}$, making use of the analytical transfer functions determined in Section 2.3. The quantity $y_{\rm end}$ is chosen to be sufficiently large so that the following integration converges to a stable value. Specifically, given the structure of our analytic solutions for the transfer functions, see Section 2.3, we conveniently split the integral in two pieces, for $y < 1$ and $y > 1$:

$$\begin{aligned}\mathcal{I}_\rho(y_{\rm end}) = {} & y_{\rm end} \int_0^1 \frac{dx_\star}{x_\star} \left[\frac{x_\star^2}{x_\star^2 + y_{\rm end}^2} |\partial_y T^{(A)}_{\rm late}|^2 + x_\star^2 |T^{(A)}_{\rm late}|^2\right] \\ & + y_{\rm end} \int_1^{y_{\rm end}} \frac{dx_\star}{x_\star} \left[\frac{x_\star^2}{x_\star^2 + y_{\rm end}^2} |\partial_y T^{(B)}_{\rm late}|^2 + x_\star^2 |T^{(B)}_{\rm late}|^2\right].\end{aligned} \tag{2.35}$$

Consider the integral in the first line of the Eq. (2.35). We first take the limit of large $y_{\rm end}$ inside the integrand function. The result is easily numerically integrated, and gives the value 0.475883. For the integral in the second line of Eq. (2.35) – since the quantity $y_{\rm end}$ appears both in the integral extreme and in the integrand – we find convenient to first rescale the integration variable from x_* to $z \equiv \frac{x_*}{y_{\rm end}}$. In this new variable, the lower extreme of integration $\frac{1}{y_{\rm end}}$ is small and can be approximated with zero. Morevoer, in the integrand function that results from this change of variable, there are terms that exhibit rapid oscillations in the $0 \leq z \leq 1$ domain, which are weighted by inverse powers of $y_{\rm end}$. We can neglect those contributions, since they average to nearly zero. Beside these contributions, the integrand contains a ratio between two polynomials in the variable $x_\star$, which once integrated gives 1.025 in the limit of large $y_{\rm end}$. The sum of the two pieces we computed is

$$\mathcal{I}_\rho = 1.50088 \simeq \frac{3}{2}, \tag{2.36}$$

a number of order one. With this result, and recalling the definition of $H_\star$ in Eq. (2.19), we obtain the following expression for the longitudinal vector energy density evaluated today

$$\rho_{A_L} = \frac{3\sigma_0}{2} \frac{H_I^2\, M^2}{8\pi^2} \left(\frac{H_{\rm eq}}{M}\right)^{3/2}, \tag{2.37}$$

where we take into account how the energy density scales with the universe evolution. The present-day DM energy density is well approximated by the formula $\rho_{\rm DM} = 3\, H_{\rm eq}^2\, M_{\rm Pl}^2/2$. Using the value $H_{\rm eq} = 3 \times 10^{-28}$ eV, we compute the ratio of these two quantities

$$\frac{\rho_{A_L}}{\rho_{\rm DM}} = \sigma_0 \left(\frac{M}{0.6 \times 10^{-6}\,{\rm eV}}\right)^{1/2} \left(\frac{H_I}{10^{14}\,{\rm GeV}}\right)^2, \tag{2.38}$$

giving a result that is in reasonable agreement [7] with [5]. We will make use of expression (2.38) in Section 4.

3 The induced gravitational wave spectrum

The vector dark matter model reviewed in the previous section leads to a longitudinal vector spectrum enhanced at scales smaller than the CMB ones, with a peak at $k \simeq k_\star \equiv a_\star M$, see Fig 1. The fluctuations of the longitudinal vector produce tensor metric perturbations (gravitational waves) at second order, in an amount quadratically proportional to their power spectrum. This leads us to investigate whether the amplifcation of the longitudinal vector in this model can result in a visible nduced GW signal. Such phenomenon is analog to what happens in models producing primordial black holes through an enhancement of curvature fluctuations, which induce a SGWB at second order in perturbations (see e.g. [40] for a comprehensive review).

Interestingly, in our context we do not need to consider deviations from standard slow roll expansion during inflation, nor the production of primordial black holes. The induced GW background is an inevitable consequence of the shape of the longitudinal vector spectrum associated with the production of vector dark matter. We investigate this subject following the approach developed in [52,53], generalising it to the case of non-adiabatic fluctuations. In the next section we discuss prospects of detection. We find that the system we consider produces an SGWB at and below nano-Hertz frequencies.

We consider mode evolution during radiation domination. Inflationary GW are transverse-traceless, spin-2 fluctuations around a FLRW background metric. They satisfy the evolution equation (using the notation of [53])

$$h''_{ij} + 2\mathcal{H}\, h'_{ij} - \nabla^2 h_{ij} \;=\; \mathcal{T}_{ij}^{\;\;lm} S_{lm}\,, \tag{3.1}$$

where S_{ij} is the longitudinal vector source, and $\mathcal{T}_{ij}^{\;\;lm}$ is the projection tensor selecting its transverse-traceless part. The GW source is extracted from the spatial components of the vector energy-momentum tensor. In our context it reads

$$\begin{aligned} S_{ij}(\tau,\mathbf{x}) \;&=\; 2M^2\,\partial_i\varphi\,\partial_j\varphi - \frac{2}{a^2(\tau)}\partial_i A_0\,\partial_j A_0 - \frac{2}{a^2(\tau)}\partial_i\varphi'\,\partial_j\varphi' \\ &\quad + \frac{2}{a^2(\tau)}\left(\partial_i A_0\,\partial_j\varphi' + \partial_j A_0\,\partial_i\varphi'\right)\,. \end{aligned} \tag{3.2}$$

It depends on the vector mass M during RD, the scalar longitudinal mode φ, and the time-component A^0 of the vector. Hence, at second order in fluctuations, the vector sources GW, which are expanded in Fourier modes as

$$h_{ij}(\tau,\mathbf{x}) \;=\; \sum_\lambda \int \frac{d^3\mathbf{k}}{(2\pi)^{3/2}}\, e^{i\mathbf{k}\cdot\mathbf{x}}\, \mathbf{e}_{ij}^{(\lambda)}(\mathbf{k})\, h_{\mathbf{k}}^{(\lambda)}\,, \tag{3.3}$$

where the sum over λ is a sum over the two GW polarizations $(+,\times)$. The polarisation tensors $\mathbf{e}_{ij}^{(\lambda)}$ are normalised as $\sum_{ij}\mathbf{e}_{ij}^{(\lambda)}\mathbf{e}_{ij}^{(\lambda')} = \delta^{\lambda\lambda'}$, and they can also be used to perform the transverse-traceless projection tensor of Eq.(3.1). The Fourier transform of the source on the right-hand

[7] There are order-one differences between our Eq. (2.38) and the analogue formula in [5]. We interpret the difference as due to our approximations in deriving the analytical transfer functions.

side of Eq. (3.1) reads [53]

$$\mathcal{T}_{ij}^{\ lm} S_{lm}(\tau,\mathbf{x}) \;=\; \sum_{\lambda} \int \frac{d^3\mathbf{k}}{(2\pi)^{3/2}}\, e^{i\mathbf{k}\cdot\mathbf{x}} \left[\mathbf{e}_{ij}^{(\lambda)}(\mathbf{k}) \mathbf{e}^{(\lambda)\, lm}(\mathbf{k})\right] S_{lm}(\mathbf{k})\,, \tag{3.4}$$

with

$$S_{lm}(\mathbf{k}) \,=\, \int \frac{d^3\mathbf{x}'}{(2\pi)^{3/2}}\, e^{-i\mathbf{k}\cdot\mathbf{x}'}\, S_{lm}(\mathbf{x}')\,. \tag{3.5}$$

Hence, the GW evolution equation (3.1) reads in Fourier space

$$h_{\mathbf{k}}^{(\lambda)\,\prime\prime} + 2\mathcal{H}\, h_{\mathbf{k}}^{(\lambda)\,\prime} + k^2 h_{\mathbf{k}}^{(\lambda)} \,=\, S_{\mathbf{k}}^{(\lambda)}(\tau)\,, \tag{3.6}$$

with the source Fourier component given by the convolution integral

$$\begin{aligned} S_{\mathbf{k}}^{(\lambda)} \;&=\; 2M^2 \int \frac{\mathsf{e}^{(\lambda)}(\mathbf{k},\tilde{\mathbf{k}})\; d^3\tilde{\mathbf{k}}}{(2\pi)^{3/2}} \\ &\quad\times\Big[\varphi_{\tilde{\mathbf{k}}}\varphi_{\mathbf{k}-\tilde{\mathbf{k}}} - \frac{1}{a^2\,M^2}\left(A_{0,\tilde{\mathbf{k}}}\, A_{0,\mathbf{k}-\tilde{\mathbf{k}}} - \varphi'_{\tilde{\mathbf{k}}}\varphi'_{\mathbf{k}-\tilde{\mathbf{k}}} - A_{0,\,\tilde{\mathbf{k}}}\,\varphi'_{\mathbf{k}-\tilde{\mathbf{k}}} + A_{0,\,\mathbf{k}-\tilde{\mathbf{k}}}\,\varphi'_{\mathbf{k}}\right)\Big]\,. \end{aligned} \tag{3.7}$$

where we introduced the combination

$$\mathsf{e}^{(\lambda)}(\mathbf{k},\tilde{\mathbf{k}}) \,\equiv\, \mathbf{e}_{ij}^{(\lambda)}(\mathbf{k})\,\tilde{k}^i\tilde{k}^j\,. \tag{3.8}$$

It is convenient to make use of the constraint equation (2.5) relating the vector time component A_0 and the longitudinal scalar φ: $A_{0\,\mathbf{k}} \,=\, \left(k^2\,\varphi'_{\mathbf{k}}\right)/(k^2+M^2a^2)$. Substituting such condition into Eq. (3.7), we find

$$S_{\mathbf{k}}^{(\lambda)} \;=\; 2\,M^2 \int \frac{\mathsf{e}^{(\lambda)}(\mathbf{k},\tilde{\mathbf{k}})\, d^3\tilde{\mathbf{k}}}{(2\pi)^{3/2}} \left[\varphi_{\tilde{\mathbf{k}}}\varphi_{\mathbf{k}-\tilde{\mathbf{k}}} - \frac{a^2\,M^2\,\varphi'_{\tilde{\mathbf{k}}}\varphi'_{\mathbf{k}-\tilde{\mathbf{k}}}}{\left(\tilde{k}^2+a^2M^2\right)\left(|\mathbf{k}-\tilde{\mathbf{k}}|^2+a^2M^2\right)}\right]\,. \tag{3.9}$$

Notice that the argument of the previous integral contains non-local contributions proportional to the inverse of momenta. They originate from the procedure of integrating out the time-like component of the vector, leading to non-canonical kinetic terms for the longitudinal mode. To proceed, we make use of the results of Section 2: the Fourier component of the longitudinal scalar φ during radiation-domination (RD) can be expressed in terms of the transfer function

$$\varphi_{\mathbf{k}}(\tau) \,=\, T(k\tau)\,\varphi_{\mathbf{k}}^{(0)}\,, \tag{3.10}$$

where the transfer function $T(k\tau)$ during RD is discussed in Section 2.2, and $\varphi_{\mathbf{k}}^{(0)}$ corresponds to the scalar primordial Fourier mode evaluated at the end of inflation. The source Fourier mode (3.9) corresponds to a convolution over primordial longitudinal modes

$$S_{\mathbf{k}}^{(\lambda)}(\tau) \;=\; 2M^2 \int \frac{\mathsf{e}^{(\lambda)}(\mathbf{k},\tilde{\mathbf{k}})\, d^3\tilde{\mathbf{k}}}{(2\pi)^{3/2}}\, \beta(\tau,k,\tilde{k})\, \varphi_{\tilde{\mathbf{k}}}^{(0)}\varphi_{\mathbf{k}-\tilde{\mathbf{k}}}^{(0)}\,, \tag{3.11}$$

weighted by a combination of transfer functions which we denote by

$$\beta(\tau,\mathbf{k},\tilde{\mathbf{k}}) \;\equiv\; T(\tilde{k}\tau)T(|\mathbf{k}-\tilde{\mathbf{k}}|\tau) - \frac{a^2\,M^2\,\tilde{k}\,|\mathbf{k}-\tilde{\mathbf{k}}|\,T'(\tilde{k}\tau)T'(|\mathbf{k}-\tilde{\mathbf{k}}|\tau)}{\left(\tilde{k}^2+a^2M^2\right)\left(|\mathbf{k}-\tilde{\mathbf{k}}|^2+a^2M^2\right)}\,, \tag{3.12}$$

where a prime indicate a derivative along the argument. We note that the combination β is invariant under the exchange $\tilde{k} \leftrightarrow |\mathbf{k}-\tilde{\mathbf{k}}|$.

After characterising its source, we can express the formal solution of the GW evolution Eq. (3.6) during RD:

$$h_{\mathbf{k}}^{(\lambda)}(\tau) \;=\; \frac{1}{a(\tau)} \int d\tau' g_k(\tau,\tau') \left[a(\tau')\, S_{\mathbf{k}}^{(\lambda)}(\tau')\right] , \tag{3.13}$$

where the g_k is the Green function (or, more appropriately, the non-distributional contribution to the Green function). During radiation domination:

$$g_k(\tau,\tau') \;=\; \frac{1}{k}\left[\sin(k\tau)\cos(k\tau') - \sin(k\tau')\cos(k\tau)\right] . \tag{3.14}$$

We consider the tensor spectrum as the sum over the two polarizations

$$\sum_\lambda \langle h_{\mathbf{k}}^{(\lambda)}(\tau) h_{\mathbf{q}}^{(\lambda)}(\tau)\rangle \;=\; (2\pi)^3\, \delta^{(3)}(\mathbf{k}+\mathbf{q})\, \frac{4\pi^2}{k^3}\, \mathcal{P}_h(k) . \tag{3.15}$$

which we rewrite as (the prime in the ensemble average indicates the correlation without the δ-function associated with momentum conservation)

$$\mathcal{P}_h(\tau,k) \;=\; \frac{1}{2}\frac{k^3}{2\pi^2} \sum_\lambda \langle h_{\mathbf{k}}^{(\lambda)}(\tau) h_{\mathbf{q}}^{(\lambda)}(\tau)\rangle' \tag{3.16}$$

$$\;=\; \frac{k^3}{4\pi^2}\frac{\sum_\lambda}{a^2(\tau)} \int d\tau_1 d\tau_2\, g_k(\tau,\tau_1)\, g_q(\tau,\tau_2)\, a(\tau_1)a(\tau_2) \langle S_{\mathbf{k}}^{(\lambda)}(\tau_1) S_{\mathbf{q}}^{(\lambda)}(\tau_2)\rangle , \tag{3.17}$$

where the two-point function of the source $S_{\mathbf{k}}$ in Fourier space reads

$$\begin{aligned}\langle S_{\mathbf{k}}^{(\lambda)}(\tau_1) S_{\mathbf{q}}^{(\lambda')}(\tau_2)\rangle \;=\; & 4M^4 \int \frac{d^3\tilde{\mathbf{k}}}{(2\pi)^{3/2}} \frac{d^3\tilde{\mathbf{q}}}{(2\pi)^{3/2}}\, \mathsf{e}^{(\lambda)}(\mathbf{k},\tilde{\mathbf{k}})\, \mathsf{e}^{(\lambda')}(\mathbf{q},\tilde{\mathbf{q}}) \\ & \times \beta(\tau_1,\mathbf{k},\tilde{\mathbf{k}})\, \beta(\tau_2,\mathbf{q},\tilde{\mathbf{q}})\, \langle \varphi_{\tilde{\mathbf{k}}}^{(0)} \varphi_{\mathbf{k}-\tilde{\mathbf{k}}}^{(0)} \varphi_{\tilde{\mathbf{q}}}^{(0)} \varphi_{\mathbf{q}-\tilde{\mathbf{q}}}^{(0)}\rangle .\end{aligned} \tag{3.18}$$

Expanding the scalar four-point function in Eq. (3.18) by means of Wick's theorem, and using the definition (2.14) of primordial longitudinal scalar spectrum, we find

$$\begin{aligned}\sum_\lambda \langle S_{\mathbf{k}}^{(\lambda)}(\tau_1) S_{\mathbf{q}}^{(\lambda)}(\tau_2)\rangle \;=\; & 8M^4 (2\pi^2)^2\, \delta^{(3)}(\mathbf{k}+\mathbf{q}) \int \frac{d^3\tilde{\mathbf{k}}}{(2\pi)^3} \left(\sum_\lambda \mathsf{e}^{(\lambda)}(\mathbf{k},\tilde{\mathbf{k}}) \mathsf{e}^{(\lambda)}(\mathbf{k},\tilde{\mathbf{k}})\right) \\ & \times \beta(\tau_1,\mathbf{k},\tilde{\mathbf{k}})\, \beta(\tau_2,\mathbf{k},\tilde{\mathbf{k}})\, \frac{\mathcal{P}_\varphi^{(0)}(\tilde{k})}{\tilde{k}^3} \frac{\mathcal{P}_\varphi^{(0)}(|\mathbf{k}-\tilde{\mathbf{k}}|)}{|\mathbf{k}-\tilde{\mathbf{k}}|^3} \\ \;=\; & 8\pi^2 M^4\, \delta^{(3)}(\mathbf{k}+\mathbf{q}) \int_0^\infty d\tilde{k} \int_{-1}^1 d\mu\, \frac{\tilde{k}^3(1-\mu^2)^2}{|\mathbf{k}-\tilde{\mathbf{k}}|^3}\, \beta(\tau_1,\mathbf{k},\tilde{\mathbf{k}})\, \beta(\tau_2,\mathbf{k},\tilde{\mathbf{k}}) \\ & \times \mathcal{P}_\varphi^{(0)}(\tilde{k}) \mathcal{P}_\varphi^{(0)}(|\mathbf{k}-\tilde{\mathbf{k}}|) ,\end{aligned} \tag{3.19}$$

where in the second equality we use $d^3\tilde{\mathbf{k}} = 2\pi\, \tilde{k}^2\, d\tilde{k}\, d\mu$, as well as properties of the combinations $\mathsf{e}^{(\lambda)}(\mathbf{k},\tilde{\mathbf{k}})$ defined in Eq. (3.8) (we note that $\mu \equiv (\mathbf{k}\cdot\tilde{\mathbf{k}})/(k\,\tilde{k})$ is the cosine of the angle between $\mathbf{k}$ and $\tilde{\mathbf{k}}$). The overall structure of the previous expression is similar to what is found in the literature for the case of GWs induced by second order adiabatic fluctuations.

To proceed, we plug the result (3.19) into the expression in Eq. (3.17). We use the variables $x_\star = k\tau_\star$ and $y = \tau/\tau_\star$ introduced in Eq. (2.21). We also change variable from $\tilde{k}$ to

$$v \equiv \frac{\tilde{k}}{k}\,. \tag{3.20}$$

Moreover, we use the following quantity u as abbreviation in next formulas (but we do not change variables in terms of it):

$$u \equiv \frac{|\mathbf{k}-\tilde{\mathbf{k}}|}{k} = \sqrt{1+v^2-2\mu v}\,, \tag{3.21}$$

In terms of these quantitites, we find the following expression for the tensor spectrum

$$\mathcal{P}_h\left(\tau = y\tau_\star, k = \frac{x_\star}{k_\star}\right) = \frac{4\,M^4\,x_\star^2}{y^2}\int_0^\infty dv\int_{-1}^1 d\mu\,\mathcal{P}_\varphi^{(0)}(u\,k)\,\mathcal{P}_\varphi^{(0)}(v\,k)\,\frac{\left(1-\mu^2\right)^2 v^3}{u^3}\,\mathcal{I}_T(y,\,x_\star)\,, \tag{3.22}$$

with

$$\begin{aligned}\mathcal{I}_T(y,\,x_\star) \equiv \Big|&\sin(x_\star y)\int_0^{y/k_\star} y_1\,dy_1\,\cos(x_\star y_1)\,\beta(y_1,x_\star,u,v)\\ &-\cos(x_\star y)\int_0^{y/k_\star} y_1\,dy_1\,\sin(x_\star y_1)\,\beta(y_1,x_\star,u,v)\Big|^2\,.\end{aligned} \tag{3.23}$$

In terms of the variables $x_\star$, y the function β of Eq. (3.12) reads

$$\beta(y_1,x_\star,u,v) = T(y_1,u\,x_\star)T(y_1,v\,x_\star) - \frac{y_1^2\,\left[\partial_{y_1}T(y_1,u\,x_\star)\right]\,\left[\partial_{y_1}T(y_1,v\,x_\star)\right]}{\left(u^2x_\star^2+y_1^2\right)\left(v^2x_\star^2+y_1^2\right)}\,. \tag{3.24}$$

The functions $\sin(x_\star y)$ and $\cos(x_\star y)$ in front of the integrals in Eq. (3.23) are rapidly oscillating. By expanding the square in Eq. (3.23) in the late time, large y limit, the cross term averages out and the square terms $\sin^2(x_\star y)$ and $\cos^2(x_\star y)$ average to $1/2$. Hence we conclude

$$\begin{aligned}\bar{\mathcal{I}}_T(x_\star,u,v) &= \frac{1}{2}\left[\left|\int_0^{y/k_\star} y_1\,dy_1\cos(x_\star y_1)\,\beta\right|^2 + \left|\int_0^{y/k_\star} y_1\,dy_1\sin(x_\star y_1)\,\beta\right|^2\right]\\ &\equiv \frac{1}{2}\,\bar{\mathcal{I}}_{cs}^2(x_\star,u,v)\end{aligned} \tag{3.25}$$

with $\bar{\mathcal{I}}_{cs}^2$ the content of the square bracket in the previous formula, and a bar indicates averaging over many periods of the oscillatory functions $\cos(x_\star y)$, $\sin(x_\star y)$. We numerically checked that the integrals in Eq. (3.25) converge for large values of y, and in our analysis we focus on such large-y regime where the integrals become independent from the value of the integral upper limits.

We now use the tensor power spectrum $\mathcal{P}_h$ of Eq. (3.22) to build the quantity $\Omega_{\rm GW}$, proportional to the gravitational energy density per log frequency interval. $\Omega_{\rm GW}$ is a standard parameter which controls the magnitude of SGWB in cosmological setting. It is related to the tensor spectrum by

$$\Omega_{\rm GW} = \frac{1}{24}\,\frac{k^2}{a^2H^2}\,\mathcal{P}_h\,. \tag{3.26}$$

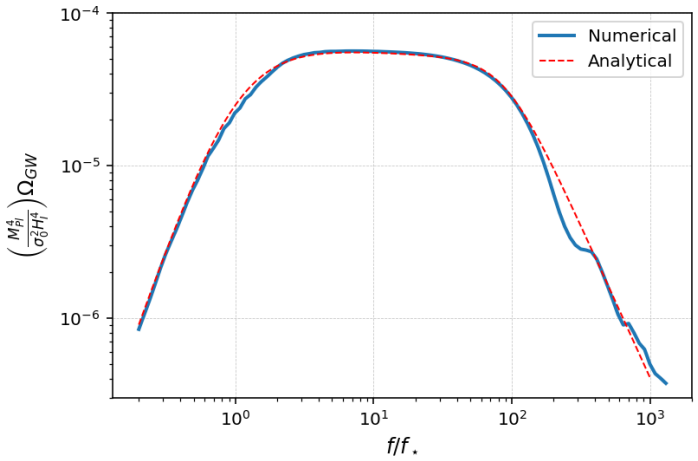

Figure 3: Representation of the GW energy density $\Omega_{\rm GW}$ of Eq. (3.31), divided by $\sigma_0^2\, H_I^4/M_{\rm Pl}^4$ (continuous blue line). We include also the analytical fitting function (3.32) (dashed red line).

During RD, $aH = 1/\tau$. We collect the previous formulas, and obtain

$$\Omega_{\rm GW}(k) \;=\; \frac{M^4}{12}\, x_\star^4 \int_0^\infty dv \int_{-1}^1 d\mu\, \bar{\mathcal{I}}^2_{cs}(x_\star,u,v)\, \mathcal{P}^{(0)}_\varphi(u\,k)\, \mathcal{P}^{(0)}_\varphi(v\,k)\, \frac{\left(1-\mu^2\right)^2 v^3}{u^3}\,, \quad (3.27)$$

where we recall $u = \sqrt{1+v^2-2\mu v}$. In view of a numerical evaluation of the integrals, it is convenient to perform another change of variables, following [54]:

$$t \;\equiv\; u+v-1 \quad , \quad s \equiv u-v\,. \quad (3.28)$$

The GW energy density becomes

$$\Omega_{\rm GW}(k) \;=\; \frac{M^4\, x_\star^4}{12} \int_0^\infty dt \int_0^1 ds \left[\frac{t(2+t)(s^2-1)}{(1-s+t)(1+s+t)}\right]^2 \bar{\mathcal{I}}^2_{cs}(x_\star,u,v)\; \mathcal{P}^{(0)}_\varphi(u\,k)\, \mathcal{P}^{(0)}_\varphi(v\,k) \quad (3.29)$$

with $u = (t+s+1)/2$, $v = (t-s+1)/2$. The integral (3.29) resembles formulas for curvature scalar induced GW – only the structure of the kernel $\bar{\mathcal{I}}^2_{cs}$ is different, compare e.g. with [54].

So far, we have not specified the amplitude of the sourcing fields. We can now make use of the results of Section 2 for the primordial spectrum $\mathcal{P}^{(0)}_\varphi$ of the longitudinal scalar mode. Such spectrum is scale invariant, and depends on the inflationary Hubble parameter H_I and vector mass M (2.16):

$$\mathcal{P}^{(0)}_\varphi(k) \;=\; \sigma_0\, \frac{H_I^2}{4\pi^2 M^2}\,. \quad (3.30)$$

We include an overall, model-dependent factor σ_0 in the previous formula. As discussed around Eq. (2.16), it aims to take into account of possible refinements of the original model [5] associated with phase transitions, non-standard evolution history or reheating after inflation, or more exotic inflationary evolution including non-minimal couplings with gravity. We do not commit on explicit scenarios, and we are going to make use of σ_0 as useful tunable parameter in our set-up. [8]

[8] A particular example able to generate a large σ_0 is discussed after Eq. (2.32).

The GW energy density results (reinstating the Planck mass, and expressing it in terms of frequency since $x_\star = k/k_\star = f/f_\star$, with $k = 2\pi f$)

$$\Omega_{\rm GW}(f) \;=\; \sigma_0^2 \left(\frac{H_I}{M_{\rm Pl}}\right)^4 \left[\frac{f^4}{192\,\pi^4\,f_\star^4}\int_0^\infty dt \int_0^1 ds \left(\frac{t(2+t)(s^2-1)}{(1-s+t)(1+s+t)}\right)^2 \bar{\mathcal{I}}^2_{cs}(f/f_\star, u, v)\right] \tag{3.31}$$

We numerically evaluate the model-independent, dimensionless quantity inside square brackets, and we represent it in Fig 3 as function of $f/f_\star$ – the fiducial frequency being $2\pi\, f_\star = a_\star\, M$ (see Eq. (2.20)). Notice that in representing $\Omega_{\rm GW}$ we factorise powers of the parameters σ_0 and of the value of the Hubble parameter during inflation.

The resulting frequency profile plotted in Fig 3 is quite broad, reflecting the scale invariant primordial spectrum for the longitudinal scalar φ as given in Eq. (3.30). We find a good analytical fit in terms of a double broken power law as

$$\left(\frac{M_{Pl}^4}{\sigma_0^2\, H_I^4}\right) \times \Omega_{\rm GW}\left(x_\star = f/f_\star\right) \;=\; 6.25\times 10^{-5}\; \frac{x_\star^{2.6}}{\left(1+x_\star^2\right)^{1.325}} \left(1+\frac{x_\star^3}{7.29\times 10^5}\right)^{-0.65} . \tag{3.32}$$

This fit intends to cover the range of frequencies $x_\star = f/f_\star$ represented in Fig 3. The maximal amplitude of the combination in the right hand side of Eq. (3.32) is of order 5×10^{-5}, and its profile remains almost constant at such maximal values in the range $3 < x_\star < 60$. The profile of $\Omega_{\rm GW}(x_\star)$ grows as $x_\star^{2.6}$ in the infrared part of the plot –for frequencies $x_\star \simeq 0.1$ or slightly larger– and it decreases as $x_\star^{-2}$ in the ultraviolet. The infrared behaviour is consistent with a change of spectral index from an $x_\star^3$ profile expected by causality arguments in the limit $x_\star \to 0$, to a milder $x_\star^{2.6}$ growth as $\Omega_{\rm GW}$ increases, and approaches the plateau at larger frequency values. The ultraviolet scaling $\Omega_{\rm GW} \simeq x_\star^{-2}$, which follows an extended plateau in frequency, is the result of our numerical integration of eq (3.31). It would be interesting to acquire an analytical understanding of such ultraviolet behavior of the GW energy density. However, the task is particular difficult due to the highly oscillator integrals entering the definition of $\mathcal{I}^2_{\rm cs}$ in Eq (3.25), which do not allow for exact solutions.

Depending on the values of σ_0, H_I, and $f_\star$ our results have different phenomenological consequences: which we explore in the next section.

4 Phenomenological consequences

We now collect the results of the previous sections and discuss their phenomenological consequences for the physics of the induced GW from longitudinal vector DM. The longitudinal vector mode A_L has a spectrum peaked around the scale $k_\star = a_\star M$, with M the vector mass during RD, while $a_\star$ is the value of the scale factor which corresponds to $H(a_\star) = M$ – see Section 2. We setting the present value of the scale factor to one, $a_0 = 1$, so that the momentum scale $k_\star$ is mapped to the frequency f_* via

$$2\pi\, f_\star \;=\; k_\star = M\, a_\star \;=\; \frac{M}{z_{\rm eq}}\left(\frac{H_{\rm eq}}{H_*}\right)^{1/2} \;=\; \frac{\sqrt{M\, H_{\rm eq}}}{z_{\rm eq}} \;=\; 4.95\;\times\; 10^{-18}\,{\rm eV}\left(\frac{M}{\rm eV}\right)^{1/2}, \tag{4.1}$$

where we make use of $H_{\rm eq} = 3\times 10^{-28}$ eV and $z_{\rm eq} = 3400$ [55]. "Converting" eV to Hertz, we get

$$f_\star \;=\; 1.2\left(\frac{M}{10^6\,{\rm eV}}\right)^{1/2} {\rm Hz}\,. \tag{4.2}$$

Actually, as we observe from Fig 3, the induced GW spectrum grows and is amplified at frequencies slightly larger than $f_\star$, acquiring its maximal values for frequencies in the order $c_0 f_\star$ with $c_0 \simeq \mathcal{O}(10)$. To proceed, we recall formula (2.38) which provides the ratio of longitudinal vector A_L versus the dark matter energy density today

$$\begin{aligned} \frac{\rho_A}{\rho_{\rm DM}} &= 12.7\,\sigma_0 \left(\frac{\rm eV}{H_{\rm eq}}\right)^{\frac{1}{2}} \left(\frac{M}{10^6\,{\rm eV}}\right)^{\frac{1}{2}} \left(\frac{H_I}{M_{\rm Pl}}\right)^2 \\ &= 5.7\times 10^{14}\,\sigma_0 \left(\frac{M}{10^6\,{\rm eV}}\right)^{\frac{1}{2}} \left(\frac{H_I}{M_{\rm Pl}}\right)^2 , \end{aligned} \tag{4.3}$$

where H_I is the Hubble parameter during inflation, and σ_0 is the model-dependent overall factor in the longitudinal scalar spectrum, see Eq. (2.16) and related discussion. Finally, the result summarized by Figure 3 indicates that the induced GW signal can obtain the maximum value

$$\Omega_{\rm GW}^{\rm max} \simeq 5\times 10^{-5}\,\sigma_0^2 \left(\frac{H_I}{M_{\rm Pl}}\right)^4 . \tag{4.4}$$

The last three equations can be employed to study the phenomenology of the model for different values of the model parameters. Let us first focus on the original model [5], for which $\sigma_0 = 1$ and we demand $\rho_A/\rho_{\rm DM} = 1$. Current CMB polarisation experiments set the bound $r \leq 0.03$ on the tensor-to-scalr ratio at large scales [56], and, correspondingly, on the scale of inflation $H_I/M_{\rm Pl} \leq 10^{-5}\sqrt{r/0.03}$. Let us choose a reference value of $H_I/M_{\rm Pl} = 10^{-6}$. Then, Eq. (4.3) indicates that the longitudinal vector coincides with the dark matter if its mass is given by $M \simeq 3$ eV. From Eq. (4.2) we then see that this mass corresponds to the characteristic GW frequency $f_\star \simeq 2\times 10^{-3}$ Hz. However, the resulting $\Omega_{\rm GW}^{\rm max} = 10^{-29}$, too small to be detected with a milli-Hertz interferometer as LISA [57]. To obtain an observable signal, we need to tune the parameter σ_0 to larger values.

Combining eqs (4.2), (4.3), and (4.4), we find the consistency condition

$$\frac{\Omega_{\rm GW}^{\rm max}}{10^{-10}} = \left(\frac{c_0}{67}\right)^2 \left(\frac{\rho_A}{\rho_{\rm DM}}\right)^2 \left(\frac{10^{-10}\,{\rm Hz}}{c_0\, f_\star}\right)^2 , \tag{4.5}$$

where we include c_0 as an overall factor in front of the frequency $f_\star$, in order to take into account that the peak $\Omega_{\rm GW}^{\rm max}$ is shifted with respect to $f_\star$: see Fig 3 and the discussions after Eq. (3.32) and Eq. (4.2). Interestingly, the relation (4.5) is *independent* of the model parameters M, H_I, and σ_0. It only relies on the hypothesis that the longitudinal scalar spectrum $\mathcal{P}_\varphi$ is scale invariant during inflation, as in Eq. (2.16). Eq. (4.5) allows us to identify the most relevant parameter regions, and, in particular, it leads to the conclusion that models that provide a signalled peaked comparatively smaller frequencies f_* have the chance to produce a comparatively larger GW signal, provided of course σ_0 is large enough. For definiteness, let us consider three representative examples:

- **Case 1: Peak at nano-Hertz scales.** We choose $f_\star = 1.5\times 10^{-10}\,$Hz and we demand that the longitudinal vector forms all of the dark matter. Then Eq. (4.5) results in the amplitude $\Omega_{\rm GW}^{\rm max} = 10^{-14}$. In turn, Eq. (4.2) indicates the vector mass $M \simeq 1.6\times 10^{-14} eV$, while Eq. (4.4) shows that the parameter σ_0 needs to satisfy $\sigma_0 \simeq 1.4\times 10^7 \left(\frac{10^{-6}\,M_p}{H_I}\right)^2$. See Fig 4, left panel, where we compare the analytical fit of $\Omega_{\rm GW}$ in Eq. (3.32) with nominal

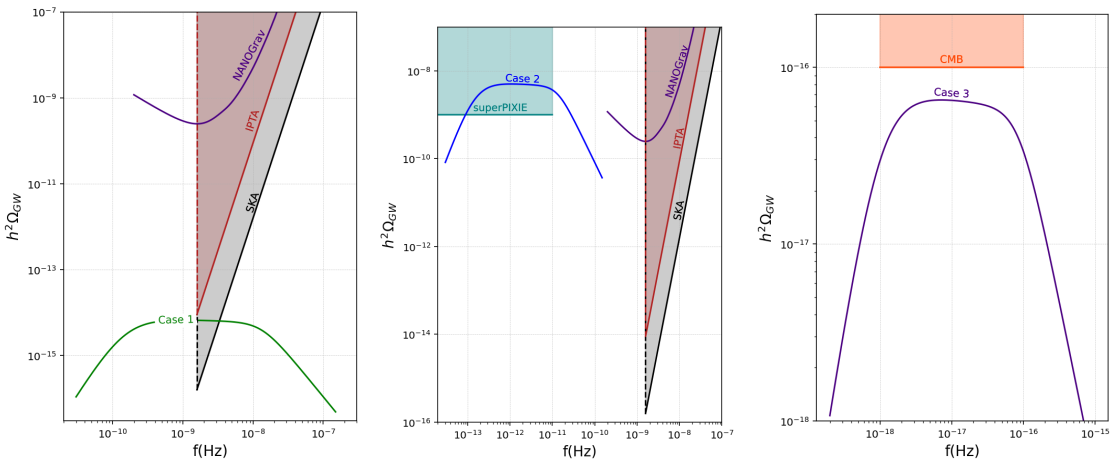

Figure 4: Representation of the three cases discussed in the main text. **Left panel**: Case 1. We take the sensitivity curves for nanoHz GW experiments from [58]. **Middle panel**: Case 2. Sensitivities curves associated to redshift space-distortion experiments are taken from [59]. **Right panel**: Case 3.

sensitivity curves of (current and future) PTA experiments, taken from [58]. In the future, SKA should be able to probe the nearly flat, central region of the $\Omega_{\rm GW}$ profile, provided that it can resolve this specific cosmological backgrounds against an astrophysical signal. Possible methods might rely on the properties of SGWB anisotropies [60–62]. Further measurements can also benefit from astrometry observations (see [63] for a review), and by the synergy of astrometry and PTA [64].

- **Case 2: Peak at intermediate scales.** Let us instead consider a peak frequency $f_\star = 1.5 \times 10^{-13}$ Hz, at intermediate scales between CMB and PTA experiments. Assuming again that the longitudinal vector forms all of the dark matter, then Eq. (4.5) results in the amplitude $\Omega_{\rm GW}^{\rm max} = 10^{-8}$. Eq. (4.2) points now to the vector mass $M = 1.5 \times 10^{-20}$ eVm which makes the light vector a 'fuzzy dark matter' candidate, see e.g. [65] for a review. From Eq. (4.4), we must require $\sigma_0 \simeq 1.4 \times 10^{10} \left(\frac{10^{-6}\, M_p}{H_I}\right)^2$. The central panel of Fig. 4 shows a representation of the analytical fit of $\Omega_{\rm GW}$ in Eq. (3.32) against the perspective sensitivity of super PIXIE – taken from [59] – an evolution of the PIXIE experiment [66–68] to measure redshift space-distortions. This result demonstrates the importance of finding methods to measure GW at intermediate frequency ranges between CMB and PTA experiments. In fact, redshift space-distortions is a promising probe for testing the SGWB induced by models of longitudinal vector DM.

- **Case 3: Peak at CMB scales.** Present bounds on the amount of primordial B-modes in CMB polarisation experiments set constraints on regions of parameter space enhancing the GW spectrum at small frequencies. For example, consider scenarios potentially able to amplify the SGWB magnitude at CMB scales $f_{\rm CMB} \simeq 10^{-18}$ Hz – corresponding to tiny vector masses $M \simeq 7 \times 10^{-31}$ eV, see Eq. (4.2). On such frequency ranges, current B-mode constraints impose $\Omega_{\rm GW}(f_{\rm CMB}) \leq (r/0.01) \times 10^{-15}$ [56]. Choosing for instance $r = 10^{-3}$ results in $\Omega_{\rm GW}^{\rm max} = 10^{-16}$, which is compatible with only a very small vector field energy density, $\rho_A/\rho_{\rm DM} \leq 7 \times 10^{-10}$, see Eq. (4.5). Future experiments as LiteBIRD can

gain further orders of magnitude in sensitivity, see e.g. [69]. It is remarkable that GW experiments are able to set so stringent constraints on tiny amounts of longitudinal vector in the DM budget.

What is particularly interesting is that the GW mechanism of production that we analysed is independent of any possible coupling of the vector A_μ to Standard Model physics. It holds even if there are no couplings at all with the Standard Model (besides gravity) – or very tiny ones [70–72]. It is interesting that the induced GW spectrum can be enhanced at frequencies below the nano-Hertz, see Eq. (4.5), setting new targets to GW experiments. Nevertheless, the requirement to get detectable signals (say values of $\Omega_{\rm GW}$ in the 10^{-10} regime) requires us to choose large values of σ_0. In principle this is possible by elaborating extensions of the original scenario [5] as discussed in the paragraphs around Eq. (2.16). Possibly, the simplest way to do so is by considering scenarios in which the vector mass deep in the inflationary era, $m_{\rm inf}$ is much smaller from the one during radiation domination, call it M. This condition changes the couplings to gravitational waves and lead to an effective value of $\sigma_0 = (M/m_{\rm inf})^2$, as commented after Eq. (2.32). Possible mechanisms related with phase transitions are discussed in [15], but more model building efforts will needed to better explore these possibilities and place them in a firmer theoretical setting.

Notice also that our formulas indicate that a sufficiently large GW signal is associated with very tiny masses for the vector boson, in regimes usually considered as fuzzy dark matter. In this case, there are other complementary gravitational probes of such instances, associated with phenomena like black hole superradiance from light vectors [73, 74]. At the astrophysics and gravitational level, it is also worth noticing that light vector bosons, like the ones considered, can form coherent fuzzy dark matter structures, and compact objects related to Proca stars [75–82]. It will be interesting to further investigate realistic particle physics constructions behind light longitudinal vector dark matter models, and understand at what extent improved GW detectors can constrain (or probe!) their predictions.

5 Outlook

We discussed a new gravitational wave probe of longitudinal vector dark matter. We computed the stochastic gravitational wave background produced at second order in fluctuations in scenarios of vector dark matter based on [5]. Our approach is similar in spirit to analysis on second order GW produced by primordial black hole models – this time applied to a particle physics dark matter set-up, and to the case of non-adiabatic fluctuations. We have shown that the GW spectrum is amplified at very small frequencies, at, or below, the nano-Hertz. Although possibly detectable at nano-Hertz scales, GW from vector dark matter constitute a particularly interesting target for very low frequency GW experiments, able to detect GW say in the region around 10^{-12} Hertz. The original DM model is very minimal – the action has only the vector mass as free parameter – but over the years several generalisations and refinements have been considered. In fact, only scenarios extending [5] lead to the hope of producing a SGWB amplitude detectable by future experiments. Models characterised by a small vector mass are more likely to lead to a detectable SGWB signal, and can be further tested by other GW probes as black hole superradiance. Hence, it would be very interesting to continue model building efforts in order to identify well motivated scenarios able to lead to a measurable GW signal. Since we only focussed

on production of GW during radiation domination, it would also be interesting to study GW production during matter domination, or in non-standard cosmologies. Also, since the vector action is relatively simple, it would also be interesting to study the effects of non-linearities.

We are setting challenging targets, both at the theoretical and at the experimental level. However, recall that the only known coupling of dark matter with Standard Model is through gravity: it might be that for some reasons such coupling is the only one chosen by Nature. In this case, further exploring the gravitational wave probe we identified – based on gravity only and in principle testable with GW experiments – is certainly a well motivated pursuit.

Acknowledgments

It is a pleasure to thank Ogan Özsoy for discussions on related topics. The work of AMB and GT is partially funded by STFC grant ST/X000648/1. M.P. acknowledges support from Istituto Nazionale di Fisica Nucleare (INFN) through the Theoretical Astroparticle Physics (TAsP) project, and from the MIUR Progetti di Ricerca di Rilevante Interesse Nazionale (PRIN) Bando 2022 - grant 20228RMX4A. For the purpose of open access, the authors have applied a Creative Commons Attribution licence to any Author Accepted Manuscript version arising. Research Data Access Statement: No new data were generated for this manuscript.

References

[1] G. Bertone, D. Hooper, and J. Silk, "Particle dark matter: Evidence, candidates and constraints," *Phys. Rept.* **405** (2005) 279–390, arXiv:hep-ph/0404175.

[2] J. L. Feng, "Dark Matter Candidates from Particle Physics and Methods of Detection," *Ann. Rev. Astron. Astrophys.* **48** (2010) 495–545, arXiv:1003.0904 [astro-ph.CO].

[3] M. Fabbrichesi, E. Gabrielli, and G. Lanfranchi, "The Dark Photon," arXiv:2005.01515 [hep-ph].

[4] D. Antypas *et al.*, "New Horizons: Scalar and Vector Ultralight Dark Matter," arXiv:2203.14915 [hep-ex].

[5] P. W. Graham, J. Mardon, and S. Rajendran, "Vector Dark Matter from Inflationary Fluctuations," *Phys. Rev. D* **93** no. 10, (2016) 103520, arXiv:1504.02102 [hep-ph].

[6] L. H. Ford, "Gravitational Particle Creation and Inflation," *Phys. Rev. D* **35** (1987) 2955.

[7] U. A. Yajnik, "GRAVITATIONAL PARTICLE PRODUCTION IN INFLATION: A FRESH LOOK," *Phys. Lett. B* **234** (1990) 271–275.

[8] D. J. H. Chung, E. W. Kolb, and A. Riotto, "Superheavy dark matter," *Phys. Rev. D* **59** (1998) 023501, arXiv:hep-ph/9802238.

[9] B. Himmetoglu, C. R. Contaldi, and M. Peloso, "Instability of the ACW model, and problems with massive vectors during inflation," *Phys. Rev. D* **79** (2009) 063517, arXiv:0812.1231 [astro-ph].

[10] M. Bastero-Gil, J. Santiago, L. Ubaldi, and R. Vega-Morales, "Vector dark matter production at the end of inflation," *JCAP* **04** (2019) 015, arXiv:1810.07208 [hep-ph].

[11] Y. Ema, K. Nakayama, and Y. Tang, "Production of purely gravitational dark matter: the case of fermion and vector boson," *JHEP* **07** (2019) 060, arXiv:1903.10973 [hep-ph].

[12] Y. Nakai, R. Namba, and Z. Wang, "Light Dark Photon Dark Matter from Inflation," *JHEP* **12** (2020) 170, arXiv:2004.10743 [hep-ph].

[13] A. Ahmed, B. Grzadkowski, and A. Socha, "Gravitational production of vector dark matter," *JHEP* **08** (2020) 059, arXiv:2005.01766 [hep-ph].

[14] E. W. Kolb and A. J. Long, "Completely dark photons from gravitational particle production during the inflationary era," *JHEP* **03** (2021) 283, arXiv:2009.03828 [astro-ph.CO].

[15] B. Salehian, M. A. Gorji, H. Firouzjahi, and S. Mukohyama, "Vector dark matter production from inflation with symmetry breaking," *Phys. Rev. D* **103** no. 6, (2021) 063526, arXiv:2010.04491 [hep-ph].

[16] T. Moroi and W. Yin, "Light Dark Matter from Inflaton Decay," *JHEP* **03** (2021) 301, arXiv:2011.09475 [hep-ph].

[17] A. Arvanitaki, S. Dimopoulos, M. Galanis, D. Racco, O. Simon, and J. O. Thompson, "Dark QED from inflation," *JHEP* **11** (2021) 106, arXiv:2108.04823 [hep-ph].

[18] T. Sato, F. Takahashi, and M. Yamada, "Gravitational production of dark photon dark matter with mass generated by the Higgs mechanism," *JCAP* **08** no. 08, (2022) 022, arXiv:2204.11896 [hep-ph].

[19] B. Barman, N. Bernal, A. Das, and R. Roshan, "Non-minimally coupled vector boson dark matter," *JCAP* **01** no. 01, (2022) 047, arXiv:2108.13447 [hep-ph].

[20] M. Redi and A. Tesi, "Dark photon Dark Matter without Stueckelberg mass," *JHEP* **10** (2022) 167, arXiv:2204.14274 [hep-ph].

[21] O. Özsoy and G. Tasinato, "Vector dark matter, inflation, and non-minimal couplings with gravity," *JCAP* **06** (2024) 003, arXiv:2310.03862 [astro-ph.CO].

[22] H. An, M. Pospelov, J. Pradler, and A. Ritz, "Direct Detection Constraints on Dark Photon Dark Matter," *Phys. Lett. B* **747** (2015) 331–338, arXiv:1412.8378 [hep-ph].

[23] S. D. McDermott and S. J. Witte, "Cosmological evolution of light dark photon dark matter," *Phys. Rev. D* **101** no. 6, (2020) 063030, arXiv:1911.05086 [hep-ph].

[24] V. S. H. Lee, A. Mitridate, T. Trickle, and K. M. Zurek, "Probing Small-Scale Power Spectra with Pulsar Timing Arrays," *JHEP* **06** (2021) 028, arXiv:2012.09857 [astro-ph.CO].

[25] M. A. Amin, M. Jain, R. Karur, and P. Mocz, "Small-scale structure in vector dark matter," *JCAP* **08** no. 08, (2022) 014, arXiv:2203.11935 [astro-ph.CO].

[26] N. Siemonsen, C. Mondino, D. Egana-Ugrinovic, J. Huang, M. Baryakhtar, and W. E. East, "Dark photon superradiance: Electrodynamics and multimessenger signals," *Phys. Rev. D* **107** no. 7, (2023) 075025, arXiv:2212.09772 [astro-ph.HE].

[27] W. E. East, "Vortex String Formation in Black Hole Superradiance of a Dark Photon with the Higgs Mechanism," *Phys. Rev. Lett.* **129** no. 14, (2022) 141103, arXiv:2205.03417 [hep-ph].

[28] A. Pierce, K. Riles, and Y. Zhao, "Searching for Dark Photon Dark Matter with Gravitational Wave Detectors," *Phys. Rev. Lett.* **121** no. 6, (2018) 061102, arXiv:1801.10161 [hep-ph].

[29] K. Nomura, A. Ito, and J. Soda, "Pulsar timing residual induced by ultralight vector dark matter," *Eur. Phys. J. C* **80** no. 5, (2020) 419, arXiv:1912.10210 [gr-qc].

[30] **PPTA** Collaboration, Y.-M. Wu, Z.-C. Chen, Q.-G. Huang, X. Zhu, N. D. R. Bhat, Y. Feng, G. Hobbs, R. N. Manchester, C. J. Russell, and R. M. Shannon, "Constraining ultralight vector dark matter with the Parkes Pulsar Timing Array second data release," *Phys. Rev. D* **106** no. 8, (2022) L081101, arXiv:2210.03880 [astro-ph.CO].

[31] C. Unal, F. R. Urban, and E. D. Kovetz, "Probing ultralight scalar, vector and tensor dark matter with pulsar timing arrays," arXiv:2209.02741 [astro-ph.CO].

[32] J.-C. Yu, Y.-H. Yao, Y. Tang, and Y.-L. Wu, "Sensitivity of Space-based Gravitational-Wave Interferometers to Ultralight Bosonic Fields and Dark Matter," arXiv:2307.09197 [gr-qc].

[33] S. Matarrese, O. Pantano, and D. Saez, "General relativistic dynamics of irrotational dust: Cosmological implications," *Phys. Rev. Lett.* **72** (1994) 320–323, arXiv:astro-ph/9310036.

[34] S. Matarrese, S. Mollerach, and M. Bruni, "Second order perturbations of the Einstein-de Sitter universe," *Phys. Rev. D* **58** (1998) 043504, arXiv:astro-ph/9707278.

[35] K. Nakamura, "Second-order gauge invariant cosmological perturbation theory: Einstein equations in terms of gauge invariant variables," *Prog. Theor. Phys.* **117** (2007) 17–74, arXiv:gr-qc/0605108.

[36] R. Saito and J. Yokoyama, "Gravitational-Wave Constraints on the Abundance of Primordial Black Holes," *Prog. Theor. Phys.* **123** (2010) 867–886, arXiv:0912.5317 [astro-ph.CO]. [Erratum: Prog.Theor.Phys. 126, 351–352 (2011)].

[37] J. R. Espinosa, D. Racco, and A. Riotto, "A Cosmological Signature of the SM Higgs Instability: Gravitational Waves," *JCAP* **1809** no. 09, (2018) 012, arXiv:1804.07732 [hep-ph].

[38] K. Inomata and T. Terada, "Gauge Independence of Induced Gravitational Waves," *Phys. Rev. D* **101** no. 2, (2020) 023523, arXiv:1912.00785 [gr-qc].

[39] R.-g. Cai, S. Pi, and M. Sasaki, "Gravitational Waves Induced by non-Gaussian Scalar Perturbations," *Phys. Rev. Lett.* **122** no. 20, (2019) 201101, arXiv:1810.11000 [astro-ph.CO].

[40] G. Domènech, "Scalar Induced Gravitational Waves Review," *Universe* **7** no. 11, (2021) 398, arXiv:2109.01398 [gr-qc].

[41] **LISA Cosmology Working Group** Collaboration, J. E. Gammal *et al.*, "Reconstructing Primordial Curvature Perturbations via Scalar-Induced Gravitational Waves with LISA," arXiv:2501.11320 [astro-ph.CO].

[42] O. Özsoy and G. Tasinato, "Inflation and Primordial Black Holes," *Universe* **9** no. 5, (2023) 203, arXiv:2301.03600 [astro-ph.CO].

[43] N. Bartolo, V. De Luca, G. Franciolini, A. Lewis, M. Peloso, and A. Riotto, "Primordial Black Hole Dark Matter: LISA Serendipity," *Phys. Rev. Lett.* **122** no. 21, (2019) 211301, arXiv:1810.12218 [astro-ph.CO].

[44] **LISA Cosmology Working Group** Collaboration, E. Bagui *et al.*, "Primordial black holes and their gravitational-wave signatures," arXiv:2310.19857 [astro-ph.CO].

[45] G. Domènech, "Cosmological gravitational waves from isocurvature fluctuations," *AAPPS Bull.* **34** no. 1, (2024) 4, arXiv:2311.02065 [gr-qc].

[46] G. Domènech, S. Passaglia, and S. Renaux-Petel, "Gravitational waves from dark matter isocurvature," *JCAP* **03** no. 03, (2022) 023, arXiv:2112.10163 [astro-ph.CO].

[47] S. Passaglia and M. Sasaki, "Primordial black holes from CDM isocurvature perturbations," *Phys. Rev. D* **105** no. 10, (2022) 103530, arXiv:2109.12824 [astro-ph.CO].

[48] A. Riotto, "Inflation and the theory of cosmological perturbations," *ICTP Lect. Notes Ser.* **14** (2003) 317–413, arXiv:hep-ph/0210162.

[49] C. Capanelli, L. Jenks, E. W. Kolb, and E. McDonough, "Gravitational production of completely dark photons with nonminimal couplings to gravity," *JHEP* **09** (2024) 071, arXiv:2405.19390 [hep-th].

[50] E. W. Kolb and A. J. Long, "Cosmological gravitational particle production and its implications for cosmological relics," *Rev. Mod. Phys.* **96** no. 4, (2024) 045005, arXiv:2312.09042 [astro-ph.CO].

[51] M. A. Gorji, M. Sasaki, and T. Suyama, "Dark matter from inflationary quantum fluctuations," arXiv:2501.03444 [astro-ph.CO].

[52] K. N. Ananda, C. Clarkson, and D. Wands, "The Cosmological gravitational wave background from primordial density perturbations," *Phys. Rev. D* **75** (2007) 123518, arXiv:gr-qc/0612013.

[53] D. Baumann, P. J. Steinhardt, K. Takahashi, and K. Ichiki, "Gravitational Wave Spectrum Induced by Primordial Scalar Perturbations," *Phys. Rev. D* **76** (2007) 084019, arXiv:hep-th/0703290.

[54] K. Kohri and T. Terada, "Semianalytic calculation of gravitational wave spectrum nonlinearly induced from primordial curvature perturbations," *Phys. Rev. D* **97** no. 12, (2018) 123532, arXiv:1804.08577 [gr-qc].

[55] **Planck** Collaboration, N. Aghanim *et al.*, "Planck 2018 results. VI. Cosmological parameters," *Astron. Astrophys.* **641** (2020) A6, arXiv:1807.06209 [astro-ph.CO]. [Erratum: Astron.Astrophys. 652, C4 (2021)].

[56] **BICEP2, Keck Array** Collaboration, P. A. R. Ade *et al.*, "BICEP2 / Keck Array x: Constraints on Primordial Gravitational Waves using Planck, WMAP, and New BICEP2/Keck Observations through the 2015 Season," *Phys. Rev. Lett.* **121** (2018) 221301, arXiv:1810.05216 [astro-ph.CO].

[57] **LISA** Collaboration, M. Colpi *et al.*, "LISA Definition Study Report," arXiv:2402.07571 [astro-ph.CO].

[58] K. Schmitz, "New Sensitivity Curves for Gravitational-Wave Signals from Cosmological Phase Transitions," *JHEP* **01** (2021) 097, arXiv:2002.04615 [hep-ph].

[59] T. Kite, A. Ravenni, S. P. Patil, and J. Chluba, "Bridging the gap: spectral distortions meet gravitational waves," *Mon. Not. Roy. Astron. Soc.* **505** no. 3, (2021) 4396–4405, arXiv:2010.00040 [astro-ph.CO].

[60] **LISA Cosmology Working Group** Collaboration, N. Bartolo *et al.*, "Probing anisotropies of the Stochastic Gravitational Wave Background with LISA," *JCAP* **11** (2022) 009, arXiv:2201.08782 [astro-ph.CO].

[61] G. Cusin and G. Tasinato, "Doppler boosting the stochastic gravitational wave background," *JCAP* **08** no. 08, (2022) 036, arXiv:2201.10464 [astro-ph.CO].

[62] J. Baker *et al.*, "High angular resolution gravitational wave astronomy," *Exper. Astron.* **51** no. 3, (2021) 1441–1470, arXiv:1908.11410 [astro-ph.HE].

[63] L. G. Book and E. E. Flanagan, "Astrometric Effects of a Stochastic Gravitational Wave Background," *Phys. Rev. D* **83** (2011) 024024, arXiv:1009.4192 [astro-ph.CO].

[64] N. M. J. Cruz, A. Malhotra, G. Tasinato, and I. Zavala, "Astrometry meets Pulsar Timing Arrays: Synergies for Gravitational Wave Detection," arXiv:2412.14010 [astro-ph.CO].

[65] E. G. M. Ferreira, "Ultra-light dark matter," *Astron. Astrophys. Rev.* **29** no. 1, (2021) 7, arXiv:2005.03254 [astro-ph.CO].

[66] A. Kogut *et al.*, "The Primordial Inflation Explorer (PIXIE): A Nulling Polarimeter for Cosmic Microwave Background Observations," *JCAP* **07** (2011) 025, arXiv:1105.2044 [astro-ph.CO].

[67] A. Kogut, M. H. Abitbol, J. Chluba, J. Delabrouille, D. Fixsen, J. C. Hill, S. P. Patil, and A. Rotti, "CMB Spectral Distortions: Status and Prospects," *Bull. Am. Astron. Soc.* **51** no. 7, (2019) 113, arXiv:1907.13195 [astro-ph.CO].

[68] J. Chluba *et al.*, "New horizons in cosmology with spectral distortions of the cosmic microwave background," *Exper. Astron.* **51** no. 3, (2021) 1515–1554, arXiv:1909.01593 [astro-ph.CO].

[69] P. Campeti, E. Komatsu, D. Poletti, and C. Baccigalupi, "Measuring the spectrum of primordial gravitational waves with CMB, PTA and Laser Interferometers," *JCAP* **01** (2021) 012, arXiv:2007.04241 [astro-ph.CO].

[70] T. Gherghetta, J. Kersten, K. Olive, and M. Pospelov, "Evaluating the price of tiny kinetic mixing," *Phys. Rev. D* **100** no. 9, (2019) 095001, arXiv:1909.00696 [hep-ph].

[71] W. E. East and J. Huang, "Dark photon vortex formation and dynamics," *JHEP* **12** (2022) 089, arXiv:2206.12432 [hep-ph].

[72] D. Cyncynates and Z. J. Weiner, "Experimental targets for dark photon dark matter," arXiv:2410.14774 [hep-ph].

[73] M. Baryakhtar, R. Lasenby, and M. Teo, "Black Hole Superradiance Signatures of Ultralight Vectors," *Phys. Rev. D* **96** no. 3, (2017) 035019, arXiv:1704.05081 [hep-ph].

[74] N. Siemonsen and W. E. East, "Gravitational wave signatures of ultralight vector bosons from black hole superradiance," *Phys. Rev. D* **101** no. 2, (2020) 024019, arXiv:1910.09476 [gr-qc].

[75] R. Brito, V. Cardoso, C. A. R. Herdeiro, and E. Radu, "Proca stars: Gravitating Bose–Einstein condensates of massive spin 1 particles," *Phys. Lett. B* **752** (2016) 291–295, arXiv:1508.05395 [gr-qc].

[76] I. Salazar Landea and F. García, "Charged Proca Stars," *Phys. Rev. D* **94** no. 10, (2016) 104006, arXiv:1608.00011 [hep-th].

[77] N. Sanchis-Gual, C. Herdeiro, E. Radu, J. C. Degollado, and J. A. Font, "Numerical evolutions of spherical Proca stars," *Phys. Rev. D* **95** no. 10, (2017) 104028, arXiv:1702.04532 [gr-qc].

[78] G. Tasinato, "Ultracompact vector stars," *Phys. Rev. D* **106** no. 4, (2022) 044022, arXiv:2205.05311 [gr-qc].

[79] B. Atkins and G. Tasinato, "Hidden conformal symmetries for black holes in modified gravity," *Phys. Rev. D* **108** no. 10, (2023) 104070, arXiv:2311.03860 [gr-qc].

[80] G. Tasinato, "Cosmic Acceleration from Abelian Symmetry Breaking," *JHEP* **04** (2014) 067, arXiv:1402.6450 [hep-th].

[81] J. Chagoya, G. Niz, and G. Tasinato, "Black Holes and Abelian Symmetry Breaking," *Class. Quant. Grav.* **33** no. 17, (2016) 175007, arXiv:1602.08697 [hep-th].

[82] J. Chagoya, G. Niz, and G. Tasinato, "Black Holes and Neutron Stars in Vector Galileons," *Class. Quant. Grav.* **34** no. 16, (2017) 165002, arXiv:1703.09555 [gr-qc].